Available online at www.sciencedirect.com
ScienceDirect
International Journal of Heat and Mass Transfer 51 (2008) 3082–3090
International Journal of HEAT and MASS TRANSFER
www.elsevier.com/locate/ijhmt

Numerical simulations of gas resonant oscillations in a closed tube using lattice Boltzmann method

Y. Wang, Y.L. He *, Q. Li, G.H. Tang

State Key Laboratory of Multiphase Flow in Power Engineering, School of Energy and Power Engineering, Xi'an Jiaotong University, Xi'an, Shaanxi 710049, China

Received 1 March 2007; received in revised form 12 August 2007
Available online 22 October 2007

Abstract

Numerical studies are presented for gas resonant oscillations in a two-dimensional closed tube using the lattice Boltzmann method. A multi-distribution function model of thermal lattice Boltzmann method is adopted in this work. The oscillating flow of the gas is generated by a plane piston at one end, and reflected by the other closed end. Both isothermal and adiabatic walls of the closed tube are considered. Boundary treatments such as moving adiabatic boundary are given in detail. The time dependent velocity, density and temperature at various locations of the tube for various frequencies and wall boundary conditions are presented. Shock waves with resonant frequency or slightly off-resonant frequencies are numerically captured. From the simulation results, the gas flow and heat transfer characteristics obtained are consistent qualitatively with those from previous simulations using conventional numerical methods.

Keywords: Lattice Boltzmann method; Gas resonant oscillations; Oscillating flow; Heat transfer

1. Introduction

The lattice Boltzmann method (LBM) was first introduced by McNamara and Zanetti [1,2], and after its development during a decade or so, it has emerged as an alternative and promising numerical approach for computational fluid dynamics (CFD) and numerical heat transfer (NHT) [3]. As a derivative of the lattice gas automata (LGA), the LBM is different from the conventional numerical methods which solving the usual macroscopic governing equations (e.g. Navier–Stokes equations) for the conserved fields. Based on the kinetic theory, the LBM simulates fluid flows by tracking the evolution of particles taking on a few discrete velocities in discrete space at discrete time steps. It is fully parallel in nature and can easily model fluid flows with complicated boundary conditions.That means the LBM provides a method to obtain streaming and heat transferring patterns for complicated systems, which are difficult to simulate with conventional numerical methods, from the microscopic and kinetic level.

The understanding of gas oscillating patterns in a closed tube is of both fundamental and practical importance. To consider a gas-filled tube driven by an oscillating plane piston at one end in the neighborhood of the fundamental resonant frequency of the gas column, periodic shock waves can be found travelling back and forth along the tube with a frequency equal to that of the oscillating piston and velocity close to that of sound [4,5]. As a result of the shock waves and oscillating flows, the heat and mass transport in a resonant tube can be enhanced dramatically compared to those beyond the resonant band.

Betchov [6] and Chester [7] constructed their theoretical models for one-dimensional resonant gas oscillations by asymptotic expansions in term of ε. Here $\varepsilon = \sqrt{\pi l/L}$ is a small parameter, l and L are the piston amplitude and tube length, respectively. Using his model, Chester was able to predict the shape and strength of the shock waves. More information about theoretical and experimental studies

* Corresponding author. Tel.: +86 29 82663851; fax: +86 29 82669106.
E-mail address: yalinghe@mail.xjtu.edu.cn (Y.L. He).

0017-9310/$ - see front matter © 2007 Published by Elsevier Ltd.
doi:10.1016/j.ijheatmasstransfer.2007.08.029

Nomenclature

a	thermal diffusivity
c	lattice streaming speed
c_s	sound speed
$\mathbf{c}_i$	particle speed
e	internal energy per unit mass
f_i	density distribution function
f_i^{eq}	equilibrium density distribution function
g_i	internal energy density distribution function
g_i^{eq}	equilibrium internal energy density distribution function
H	width of the tube
l	piston amplitude
L	length of the tube
N_x	lattice numbers at x direction
N_y	lattice numbers at y direction
p	pressure
p_0	pressure in the initial state
$\mathbf{q}$	heat flux
$\mathbf{r}$	coordinate vector
R	gas constant
t	time
Δt	time increment
T	temperature
T_0	characteristic temperature, temperature in the initial state
u	x component of the velocity
$\mathbf{u}$	velocity
w_i	weighting coefficient in f_i^{eq} and g_i^{eq}
Δx	lattice spacing
Z_i	effect of viscous heating

Greek symbols

ε	parameter defined as $\varepsilon = \sqrt{\pi l/L}$
ν	kinetic viscosity
ρ	density
ρ_0	density in the initial state
$\mathbf{\Pi}$	stress tensor
τ_f	momentum relaxation time
τ_g	internal energy relaxation time
ω	circular frequency
Ω	fundamental resonant frequency

Subscripts

i	direction
x, y	directions

Superscript

eq	equilibrium

on resonant oscillations can be found from the review of Ilgamov et al. [8] and the references . In Ref. [8], Ilgamov et al. found that the discrepancy between theory and experiments increases with the increase of ε, and concluded that all existing theories are unsatisfactory when $\varepsilon \geqslant 0.1$.

Specially, some theoretical and experimental studies aimed at the thermoacoustic effects of the resonant tube. Merkli and Thomann [9,10] investigated the transition from laminar gas motion to a turbulent one, and found the development of temperature and pressure gradients along the resonant tube. Goldshtein et al. [11] derived a model of inviscid resonant gas oscillations with an accuracy of ε^2. With their model, such phenomena observed in experiments as spatial gradients of time-averaged gas temperature and pressure can be predicted. However, the agreement between theory and experiment of their model at large ε remains rather poor [5]. Gopinath et al. [12] investigated theoretically the problem of thermoacoustic streaming in a resonant channel, and clarified the origin of the time-averaged temperature stratification.

At present, there are a few numerical simulations of gas oscillations in resonant tubes. However, most simulations are restricted to solving one-dimensional non-linear Lagrangian wave equations [13–15], although a more general two-dimensional simulation would be more attractive. This is because the appearance of non-linear shock waves in resonant oscillations and the small Mach number of the gas flow require a high-resolution numerical scheme and a large computing resource.

Most recently, Tang and Cheng [16] solved the two-dimensional gas resonant oscillation in a cylindrical tube with $\varepsilon = 0.077$ by a new finite volume method with second-order kinetic flux-vector splitting scheme for convective terms, and a third-order Runge-Kutta method for the time evolution. They claimed that their numerical results are similar to those from previous studies. Alexeev and Gutfinger [5] investigated the two-dimensional turbulent gas oscillations and acoustic streaming in resonant tubes with a finite-difference algorithm supplemented by a two-equation Wilcox turbulent model, and found that the direction of gas streaming at resonance is opposite to that in non-resonant oscillations.

On the other hand, it is well known that the LBM is capable of simulating acoustic problems [17–20]. Considering its advantages mentioned above, we adopted the LBM to study the flow and heat transfer characteristics systematically in a thermoacoustic refrigerator. In order to simulate the gas resonant oscillations in a closed tube, using the LBM is an unavoidable step in this study. However, there is no open literature in this field. In the present work, numerical simulations are performed for gas resonant oscillating phenomena in a closed tube using the LBM. Both isothermal and adiabatic walls are considered in simulations. From the numerical results, shock waves with reso-

nant frequency or slightly off-resonant frequencies are numerically captured. The time dependent velocity, density, and temperature at various locations of the tube for various frequencies and wall boundary conditions are presented. The gas flow and heat transfer characteristics obtained are consistent qualitatively with those from previous simulations using conventional numerical methods.

In the following sections, the LBM model adopted in this work is introduced in Section 2. In Section 3, we give details of the boundary conditions of the LBM. Section 4 introduces the physical model of the gas oscillations in a tube and presents the results obtained from the LBM simulations. Finally, a brief conclusion is given in Section 5.

2. The thermal LBM

At present, one of the most popular categories of the thermal LBM (TLBM) models, which are developed to treat heat transfer, are the multi-distribution function models [21–28]. In these multi-distribution function models, an independent internal energy or temperature density distribution function, besides the density distribution function, is introduced to solve the temperature field. Compared with other categories, such as the multi-speed models [29–31], these multi-distribution function models have a better numerical stability.

The TLBM model originally derived by He et al. [22] is used in this study. In this model, the temperature field is solved with a separate internal energy density distribution function g_i, which is different from the density distribution function f_i used for solving velocity field. The discrete distribution functions obey a set of lattice Bhatnagar–Gross–Krook (BGK) equations

$$\overline{f}_i(\mathbf{r}+\mathbf{c}_i\Delta t, t+\Delta t)-\overline{f}_i(\mathbf{r},t) = -\frac{\Delta t}{\tau_f+0.5\Delta t}\left[\overline{f}_i(\mathbf{r},t)-f_i^{\mathrm{eq}}(\mathbf{r},t)\right] \tag{1}$$

$$\overline{g}_i(\mathbf{r}+\mathbf{c}_i\Delta t, t+\Delta t)-\overline{g}_i(\mathbf{r},t) = -\frac{\Delta t}{\tau_g+0.5\Delta t}[\overline{g}_i(\mathbf{r},t)-g_i^{\mathrm{eq}}(\mathbf{r},t)]-\frac{\tau_g\Delta t}{\tau_g+0.5\Delta t}f_iZ_i \tag{2}$$

The variables $\overline{f}_i$ and $\overline{g}_i$ are defined as

$$\overline{f}_i = f_i+\frac{0.5\Delta t}{\tau_f}(f_i-f_i^{\mathrm{eq}}) \tag{3}$$

$$\overline{g}_i = g_i+\frac{0.5\Delta t}{\tau_g}(g_i-g_i^{\mathrm{eq}})+\frac{\Delta t}{2}f_iZ_i \tag{4}$$

where f_i^{eq} and g_i^{eq} are the equilibrium density distribution function and internal energy density distribution function respectively; $\mathbf{c}_i$ is the lattice velocity and i denotes the lattice direction; t and Δt are the time and time increment, respectively; $\mathbf{r}$ is the coordinate vector; τ_f and τ_g are the momentum and internal energy relaxation time, respectively. The term $Z_i=(\mathbf{c}_i-\mathbf{u})\cdot[\partial\mathbf{u}/\partial t+(\mathbf{c}_i\cdot\nabla)\mathbf{u}]$ represents the effect of viscous heating, and is discretized as [32]:

$$Z_i = \frac{[\mathbf{c}_i-\mathbf{u}(\mathbf{r},t)]\cdot[\mathbf{u}(\mathbf{r}+\mathbf{c}_i\Delta t, t+\Delta t)-\mathbf{u}(\mathbf{r},t)]}{\Delta t} \tag{5}$$

where $\mathbf{u}$ is the velocity. Moreover, we emphasize that the viscous heat dissipation and compression work done by the pressure can be effectively treated in this model. This is the very reason we choose He et al.'s model in this study. As the flows considered here are viscid and compressible with small Mach number, the viscous heat dissipation and compression work can not be neglected.

For the two-dimensional nine-directional (D2Q9) lattice with streaming speed $c=\sqrt{3RT_0}$, where R and T_0 are the specific gas constant and the characteristic temperature, respectively, the equilibrium density distributions are chosen as follows:

$$f_i^{\mathrm{eq}} = \rho w_i[1+s_i(\mathbf{u})], \quad i=0,\ldots,8 \tag{6}$$

$$g_0^{\mathrm{eq}} = w_0\rho e s_0(\mathbf{u}) \tag{7}$$

$$g_i^{\mathrm{eq}} = w_i\rho e\left[\frac{3}{2}+s_i(\mathbf{u})-\frac{3(\mathbf{c}_i\cdot\mathbf{u})}{2c^2}\right], \quad i=1,2,3,4 \tag{8}$$

$$g_i^{\mathrm{eq}} = w_i\rho e\left[3+s_i(\mathbf{u})+\frac{3(\mathbf{c}_i\cdot\mathbf{u})}{c^2}\right], \quad i=5,6,7,8 \tag{9}$$

$$\mathbf{c}_i = \begin{cases} 0, i=0 \\ c\left\{\cos\left[(i-1)\frac{\pi}{2}\right], \sin\left[(i-1)\frac{\pi}{2}\right]\right\}, \\ \quad i=1,2,3,4 \\ \sqrt{2}c\left\{\cos[(i-5)\frac{\pi}{2}+\frac{\pi}{4}], \sin\left[(i-5)\frac{\pi}{2}+\frac{\pi}{4}\right]\right\}, \\ \quad i=5,6,7,8 \end{cases} \tag{10}$$

$$s_i(\mathbf{u}) = \frac{3(\mathbf{c}_i\cdot\mathbf{u})}{c^2}+\frac{9(\mathbf{c}_i\cdot\mathbf{u})^2}{2c^4}-\frac{3(\mathbf{u}\cdot\mathbf{u})}{2c^2}, \quad i=0,\ldots,8 \tag{11}$$

where w_i is the weighting coefficient and $w_0=4/9$, $w_i=1/9$ for $i=1,2,3,4$ and $w_i=1/36$ for $i=5,6,7,8$. The internal energy density is $\rho e=\rho RT$ (in 2D).

The macroscopic density ρ, velocity $\mathbf{u}$, internal energy per unit mass e, and heat flux $\mathbf{q}$, are defined in terms of the particle distribution functions as follows:

$$\rho = \sum_i \overline{f}_i \tag{12}$$

$$\rho\mathbf{u} = \sum_i \overline{f}_i\mathbf{c}_i \tag{13}$$

$$\rho e = \sum_i \overline{g}_i-\frac{\Delta t}{2}\sum_i f_iZ_i \tag{14}$$

$$\mathbf{q} = \left(\sum_i \mathbf{c}_i\overline{g}_i-\rho e\mathbf{u}-\frac{\Delta t}{2}\sum_i \mathbf{c}_if_iZ_i\right)\frac{\tau_g}{\tau_g+0.5\Delta t} \tag{15}$$

Through the multi-scaling expansion, the continuity, momentum and energy equations at the Navier–Stokes level can be derived form Eqs. (1) and (2):

$$\frac{\partial\rho}{\partial t}+\nabla\cdot(\rho\mathbf{u})=0 \tag{16}$$

$$\frac{\partial(\rho\mathbf{u})}{\partial t}+\nabla\cdot(\rho\mathbf{u}\mathbf{u}) = -\nabla p+\nabla\cdot\mathbf{\Pi} \tag{17}$$

$$\frac{\partial(\rho e)}{\partial t}+\nabla\cdot(\rho\mathbf{u}e) = \nabla\cdot(\rho a\nabla e)+\mathbf{\Pi}:\nabla\mathbf{u}-p\nabla\cdot\mathbf{u} \tag{18}$$

where the kinetic viscosity v, the pressure p, the thermal diffusivity a and the stress tensor $\mathbf{\Pi}$ are defined as $v = \tau_f RT_0$, $p = \rho RT_0$, $a = 2\tau_g RT_0$ and $\mathbf{\Pi} = \rho v(\nabla\mathbf{u} + \mathbf{u}\nabla)$, respectively.

Finally, we denote that the lattice Boltzmann equations (Eqs. (1) and (2)) used in the standard lattice Boltzmann method with streaming-collision procedure can be viewed as a special discrete form of the discrete velocity Boltzmann equation with second-order in time and space.

3. Boundary conditions

As proposed by Guo et al. [33] and Tang et al. [25], both for the velocity and temperature boundary conditions at the wall, the distribution functions are decomposed into their equilibrium and nonequilibrium parts. The equilibrium parts are defined as Eqs. (6)–(9). It should be noted that if there are some unknown parameters (e.g. the density) at the boundary nodes, we will replace them by the corresponding parameters at the nearest nodes of the interior fluid. The nonequilibrium parts are approximated with a first-order extrapolation of the nonequilibrium parts of the distribution functions at the nearest nodes of the interior fluid. It is demonstrated that the accuracy of these boundary conditions are indeed of second-order [25].

As an example shown in Fig. 1 for the D2Q9 lattice, the *BOD* line lies at the boundary, and the nodes E, A and F are those lying in the fluid. The post-collision distributions at the boundary node O, can be written as

$$\overline{f}_i^{+}(O,t) = f_i^{\mathrm{eq}}(\rho(A),\mathbf{u}(O),t) + (1-\tilde{\tau}_f)[f_i(A,t) - f_i^{\mathrm{eq}}(A,t)] \tag{19}$$

$$\overline{g}_i^{+}(O,t) = g_i^{\mathrm{eq}}(\rho(A),\mathbf{u}(O),T(O),t) + (1-\tilde{\tau}_g)[g_i(A,t) - g_i^{\mathrm{eq}}(A,t)] - \tilde{\tau}_g\tau_g f_i(O)Z_i(O) \tag{20}$$

where $\tilde{\tau}_f$ is used to replace $\Delta t/(\tau_f + 0.5\Delta t)$ for simplicity, and $\tilde{\tau}_g$ to replace $\Delta t/(\tau_g + 0.5\Delta t)$. Taking the expression of $\overline{f}_i^{+}(O,t)$ as an example, $f_i^{\mathrm{eq}}(\rho(A),\mathbf{u}(O),t)$ and $(f_i(A,t) - f_i^{\mathrm{eq}}(A,t))$ are the equilibrium and nonequilibrium parts of the density distribution, respectively.

For an adiabatic wall, which means $T(O)$ is unknown, an additional treatment of $T(O)$ is needed. Similar to the Neumann boundary proposed in Ref. [25], here we give the expression of the moving adiabatic boundary, where the heat flux $\mathbf{q}(O)$ is zero and the velocity $\mathbf{u}(O)$ not zero. We can use the expression of $\mathbf{q}$ (see Eq. (15)), together with Eqs. (7)–(9) and (20) to obtain the wall temperature $T(O)$

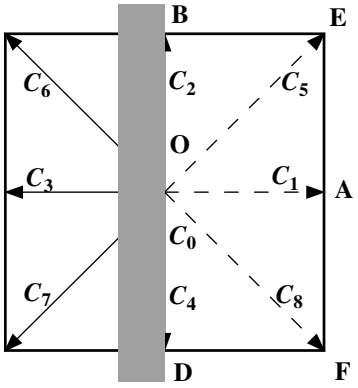

Fig. 1. Schematic plot of the boundary condition.

where $[\mathbf{c}_i f_i Z_i]_x$ and u are the x component of the vector $\mathbf{c}_i f_i Z_i$ and $\mathbf{u}$, respectively. Then, combining with Eq. (20), we can yield the post-collision distributions at the moving adiabatic boundary nodes.

4. Results and discussion

In this paper, the LBM is adopted to simulate the gas resonant oscillations in a two-dimensional closed tube composed by two parallel plates (Fig. 2). The oscillating flow is generated by a plane piston at left end ($x = 0$) with the velocity $u_0 = l\omega\sin(\omega t)$, and reflected by the other closed end ($x = L$). Here l and ω are the oscillatory amplitude and circular frequency, respectively. The initial parameters of the gas-filled in the closed tube are given as density ρ_0, pressure p_0 and temperature T_0. Therefore, the corresponding sound speed of the gas is $c_s = \sqrt{RT_0}$ in LBM, and the fundamental resonant frequency of the tube is $\Omega = \pi c_s/L$.

No-slip boundary conditions for the gas velocity are imposed at all solid walls. Both isothermal and adiabatic walls are considered. Corresponding treatments are described in Section 3. For saving computing resource, a

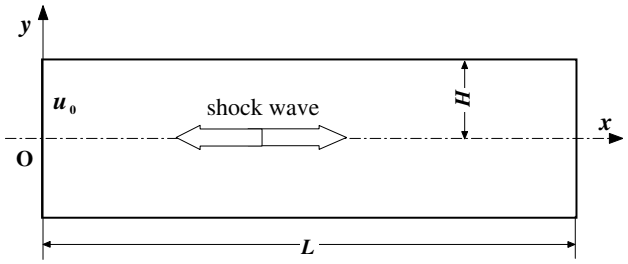

Fig. 2. Schematic description of the resonant tube.

$$T(O) = \frac{\frac{\Delta t}{2}\sum_i [\mathbf{c}_i f_i(O)Z_i(O)]_x + \sum_{i=3,6,7}\mathbf{c}_i\overline{g}_i - \sum_{i=1,5,8}\left\{(1-\tilde{\tau}_g)[g_i(A,t) - g_i^{\mathrm{eq}}(A,t)] - \tilde{\tau}_g\tau_g f_i(O)Z_i(O)\right\}}{R\rho(A)\left\{w_1\left[\frac{3}{2} + s_1(\mathbf{u}(O)) - \frac{3(\mathbf{c}_1\cdot\mathbf{u}(O))}{2c^2}\right] + \sum_{i=5,8} w_i\left[3 + s_i(\mathbf{u}(O)) + \frac{3(\mathbf{c}_i\cdot\mathbf{u}(O))}{c^2}\right] - u(O)\right\}} \tag{21}$$

half-domain ($0 \leqslant x \leqslant L$, $0 \leqslant y \leqslant H$) is considered during simulation. Mirror symmetric boundary conditions [34,35] are imposed at $y = 0$. The gas oscillations are examined for $\varepsilon = \sqrt{\pi l/L} = \sqrt{l\omega/c_s} = \sqrt{0.008}$. The frequency range to be considered is in the neighborhood of Ω.

In simulations, square lattice is adopted. The lattice numbers are N_x and N_y at x and y directions, respectively. Fig. 3 shows the mesh refinement study of the density near the closed end ($x/L = 0.99$, $y/H = 0$) with the isothermal wall at $\omega/\Omega = 1$, where the dimensionless time $tc_s/2L$ means the ordinal number of the oscillation period. It should be noted that the periodically steady state of the gas column has already been reached at $tc_s/2L = 40$ in this study. From Fig. 3, it can be found that the discrepancy between $N_x \times N_y = 1000 \times 100$ and 1200×120 is not significant. Thus it may be deduced that $N_x \times N_y = 1000 \times 100$ is competent for the problems of this paper. This is used in computing the results presented. Moreover, in order to obtained the same physical size $L \times H$ from the different lattice sizes $N_x \times N_y$, v and a increase linearly with the increase of the lattice numbers. For instance, with $c_s = 1/\sqrt{3}$, v is set as 0.06 and 0.1 for $N_x \times N_y = 600 \times 60$ and 1000×100, respectively. And the thermal diffusivity is set as $a = v/Pr = v/0.7$, where Pr is the Prandtl number.

Figs. 4 and 5 present the time dependent density at the middle point of the tube ($x/L = 0.5$, $y/H = 0$) with the isothermal walls for various frequencies in the neighborhood of Ω. Fig. 4 refers to the entire interval $0 \leqslant tc_s/2L \leqslant 50$ and provides an idea of the overall processes. From Fig. 4, it can be observed that rapid increases in the oscillation amplitudes take place at all frequencies presented over an initial period. Then, oscillations of the density are hardly visible, especially for the frequencies close to the fundamental resonant frequency. Moreover, it can be found that the periodically steady states of the system have already been reached at $tc_s/2L = 25$ for all the isothermal cases presented. Because of the influence of the walls and the gas viscosity, the maximal amplitude of the oscillating density corresponds to $\omega/\Omega = 0.97$ instead of 1.0.

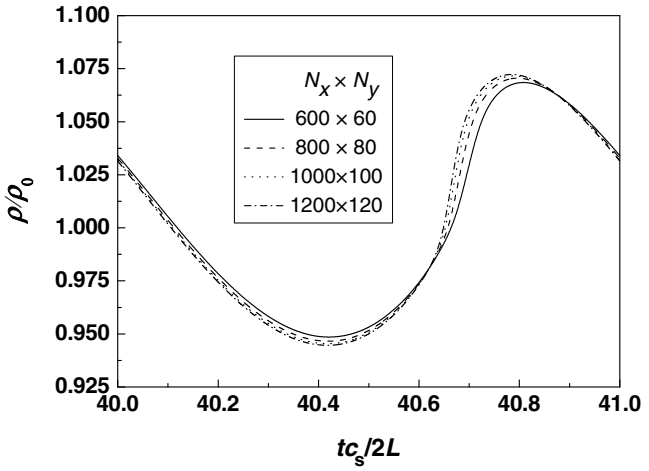

Fig. 3. Mesh refinement study of the time dependent density near the closed end of the tube ($x/L = 0.99$, $y/H = 0$) with the isothermal walls. $\omega/\Omega = 1$.

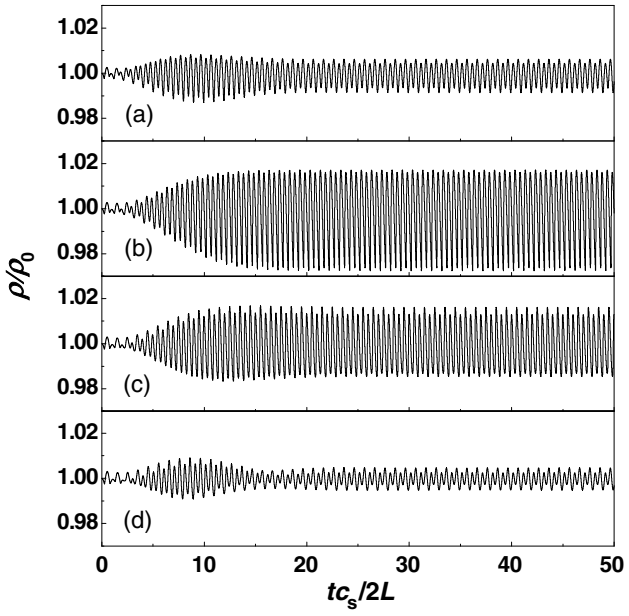

Fig. 4. Time histories of the density at the middle point of the tube ($x/L = 0.5$, $y/H = 0$) with the isothermal walls for four frequencies in the neighborhood of Ω. (a) $\omega/\Omega = 0.93$, (b) $\omega/\Omega = 0.97$, (c) $\omega/\Omega = 1.0$ and (d) $\omega/\Omega = 1.03$.

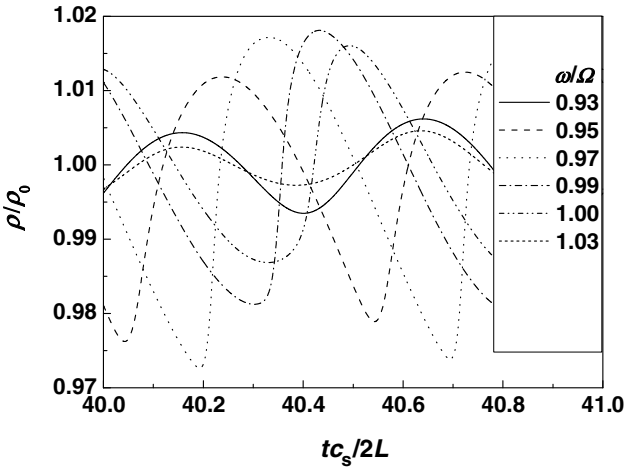

Fig. 5. Temporal variations of the density at the middle point of the tube ($x/L = 0.5$, $y/H = 0$) with the isothermal walls for six frequencies in the neighborhood of Ω under the periodically steady states.

Fig. 5 calls attention to the oscillation forms of the density after the periodically steady states have been reached. It may be seen from Fig. 5 that the waveforms of the density transform with the change of the frequencies. In particular, when the frequencies depart from the resonance ($\omega/\Omega = 0.95$ and 1.0), the amplitudes of the density oscillation become smaller, and the shock waves generated inside the tube become weaker. When the frequencies are far away from the resonant frequency ($\omega/\Omega = 0.93$ and 1.03), the waveforms are approximately sine waves. It should be

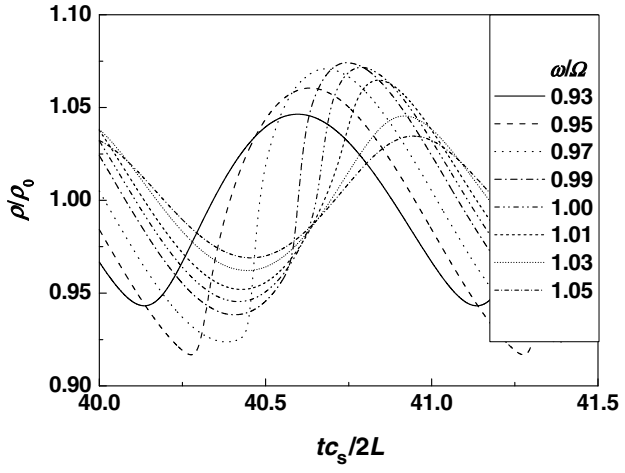

Fig. 6. Oscillation waveforms near the closed end of the tube ($x/L = 0.99$, $y/H = 0$) with the isothermal walls for eight frequencies in the neighborhood of Ω.

noted that because of the symmetry of geometry, two wave crests of the density in one oscillation period are observed at the midpoint of the tube.

For comparison with the results in references, Fig. 6 gives the temporal variations of the density near the closed end ($x/L = 0.99$, $y/H = 0$) for eight frequencies in the neighborhood of Ω. It can be seen that the transformation trend of the oscillation forms of the density near the closed tube is similar to that at the middle of the tube mentioned above. Moreover, the pre-resonant oscillation form (such as $\omega/\Omega = 0.95$) is distinctive in that it is adjacent to the maximum over a period after a pulse-type jump, however, the post-resonant oscillation form (such as $\omega/\Omega = 1.01$) has a maximum immediately after the jump. These results are very similar to those shown in Ref. [4,10,36]. As $p = \rho RT_0$ mentioned in Section 2, we have $p/p_0 = \rho/\rho_0$ for He et al.'s model. In other words, the temporal variations of the nondimensional pressure are same as those of the nondimensional density. The state equation $p = \rho RT$ can be recovered accurately in some recently proposed compressible LBM models [37].

Figs. 7 and 8 show the temporal variations of the axial ($y/H = 0$) velocity, density and temperature at two locations of the tube ($x/L = 0.01$ and 0.99) with isothermal walls at $\omega/\Omega = 0.97$. From Fig. 7, it can be seen that the waveform of velocity is almost sinusoidal with the piston movement, and a sudden pulse-type change occurs when the shock wave travels through this location ($x/L = 0.01$, $y/H = 0$). Therefore, the parameters such as density and temperature increase sharply at the same time. Corresponding temporal parameters near the closed end of the tube ($x/L = 0.99$, $y/H = 0$) are presented in Fig. 8. Similar phenomena are presented in Figs. 3–5 for adiabatic walls in Ref. [16].

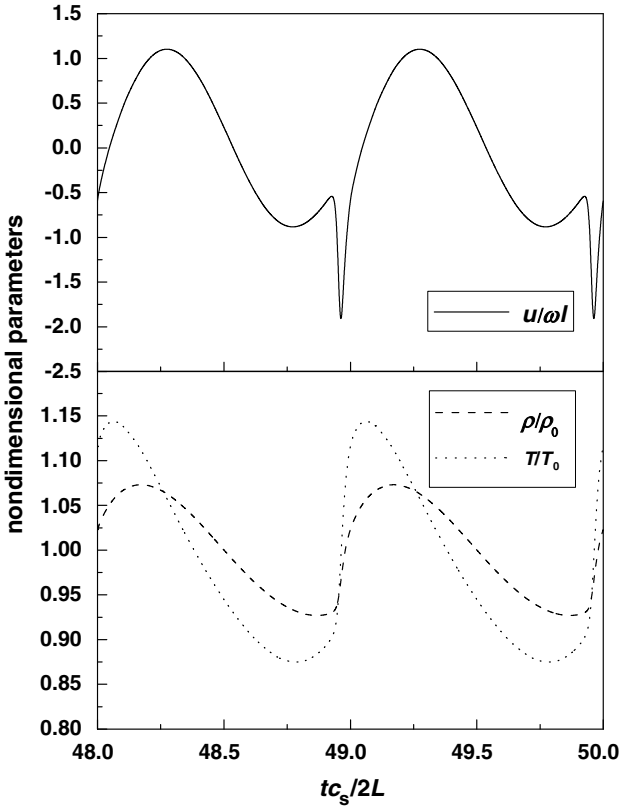

Fig. 7. Temporal variations of the axial velocity, density and temperature near the piston ($x/L = 0.01$, $y/H = 0$) with isothermal walls. $\omega/\Omega = 0.97$.

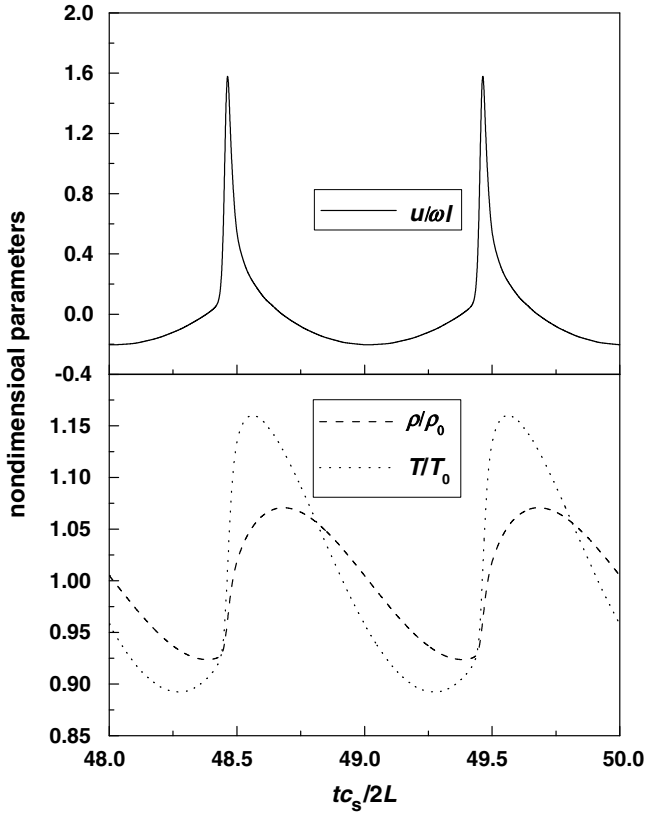

Fig. 8. Temporal variations of the axial velocity, density and temperature near the closed end of the tube ($x/L = 0.99$, $y/H = 0$) with isothermal walls. $\omega/\Omega = 0.97$.

Temporal variations of the velocity and temperature at $x/L = 0.5$ and two vertical positions ($y/H = 0$ and 0.9) with isothermal walls at $\omega/\Omega = 0.97$ are presented in Fig. 9. It can be seen from Fig. 9 that the amplitudes of both the velocity and temperature oscillations near the wall ($y/H = 0.9$) are smaller than those in the core flow region ($y/H = 0$), whenas the phase differences of the velocity and temperature oscillations between these two regions are approximate zero. In comparison of Figs. 7–9 (only for the curves of $y/H = 0$), the amplitudes of the temperature near the piston and the closed end of the tube are almost the same, and the amplitudes of these oscillations are larger than that at the midpoint of the tube. However, the amplitudes of the velocity near the piston and the closed of the tube are much smaller than that at the midpoint of the tube.

Fig. 10a shows the velocity profiles at $\omega t = 3\pi/2$ in interval $49 \leqslant tc_s/2L \leqslant 50$ and various cross sections with isothermal walls at $\omega/\Omega = 1$. Fig. 10b shows the development of temperature profiles at $x/L = 0.75$ in interval $49 \leqslant tc_s/2L \leqslant 50$ with isothermal walls at $\omega/\Omega = 1$. As shown in Fig. 10, annular effects exist both in the velocity and temperature profiles. It is interesting to note that for the curve $x/L = 7/8$ in Fig. 10a, the direction of the velocity near the wall is opposite to that in the core flow region. This is the characteristic of oscillating flow.

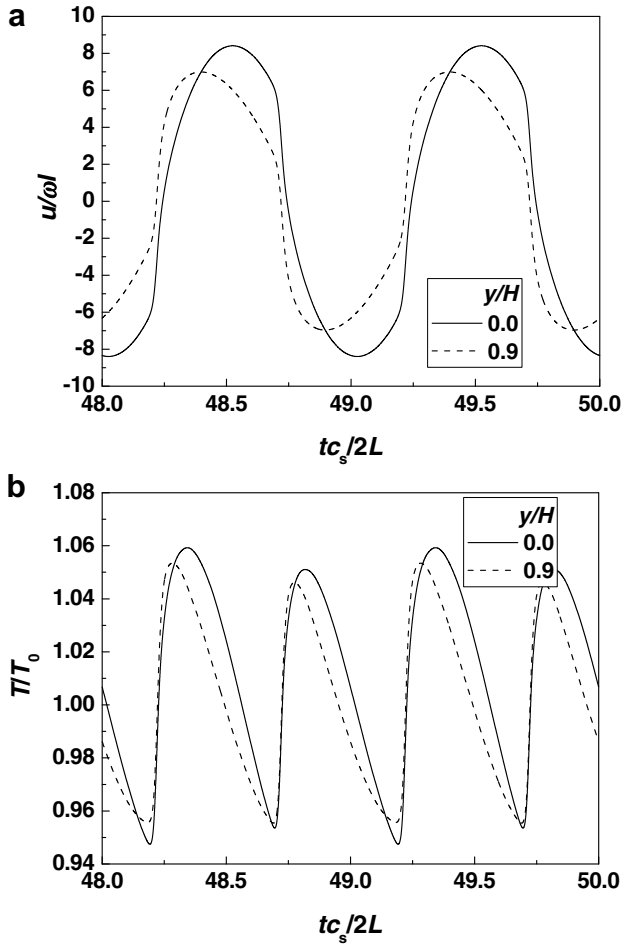

Fig. 9. Temporal variations of the (a) velocity and (b) temperature at $x/L = 0.5$ and two vertical positions ($y/H = 0$ and 0.9) with isothermal walls. $\omega/\Omega = 0.97$.

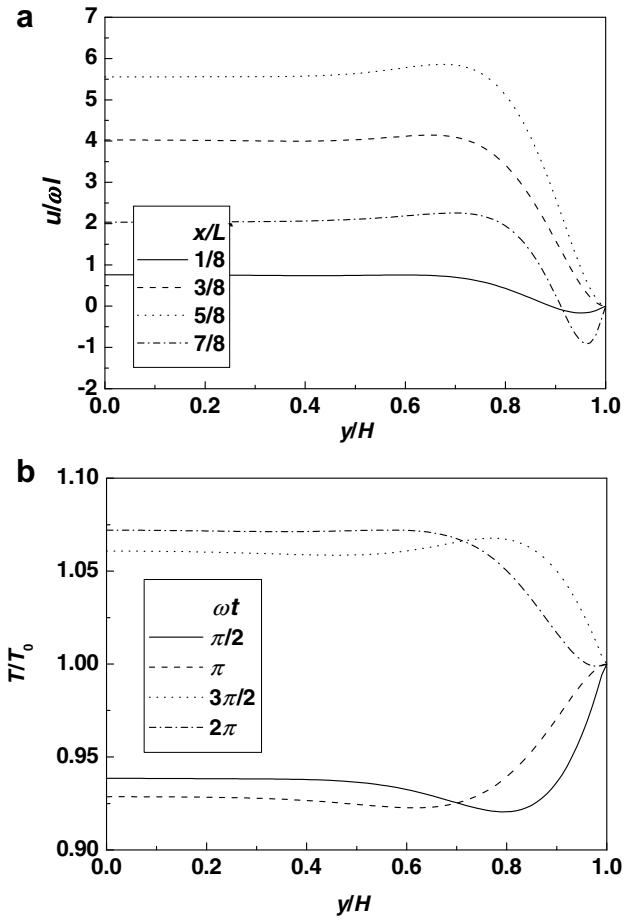

Fig. 10. (a) Velocity profiles at $\omega t = 3\pi/2$ and various cross sections and (b) development of temperature profiles at $x/L = 0.75$ with isothermal walls. $\omega/\Omega = 1$, $49 \leqslant tc_s/2L \leqslant 50$.

Similar wave structures inside the tube for adiabatic walls compared with the isothermal case are obtained numerically (not shown here). However, as there is no heat loss from the fluid to the walls for the adiabatic case, some special phenomena about the time dependent temperatures are observed. A detailed description of the temperatures in interval $0 \leqslant tc_s/2L \leqslant 100$ can be found in Fig. 11, where the temperatures used were averaged over one oscillation period. It is seen that the temperatures increase with the time, because the state of the gas column is essentially periodically unsteady. The maximal deviation from T_0 corresponds to $\omega/\Omega = 0.97$.

Fig. 12a presents the velocity profiles at $\omega t = 2\pi$ in interval $99 \leqslant tc_s/2L \leqslant 100$ and various cross sections with adiabatic walls at $\omega/\Omega = 1$. It shows that annual effects also exist in the velocity profiles of the adiabatic case. Fig. 12b presents the development of temperature profiles at $x/L = 0.625$ with adiabatic walls at $\omega/\Omega = 1$. It shows

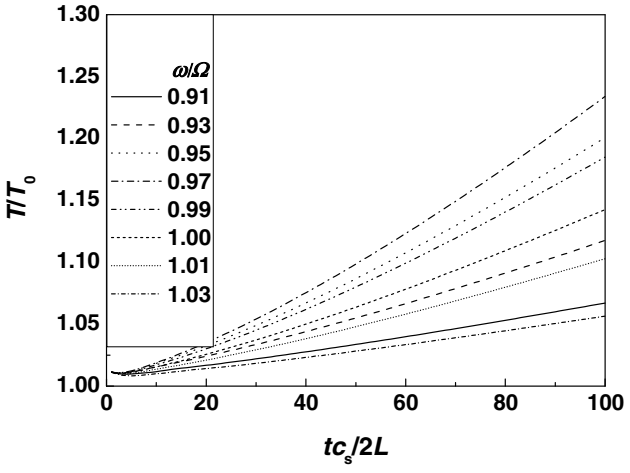

Fig. 11. The time dependencies of the period averaging temperatures near the closed end of the tube ($x/L = 0.99$, $y/H = 0$) with adiabatic walls for eight frequencies in the neighborhood of Ω.

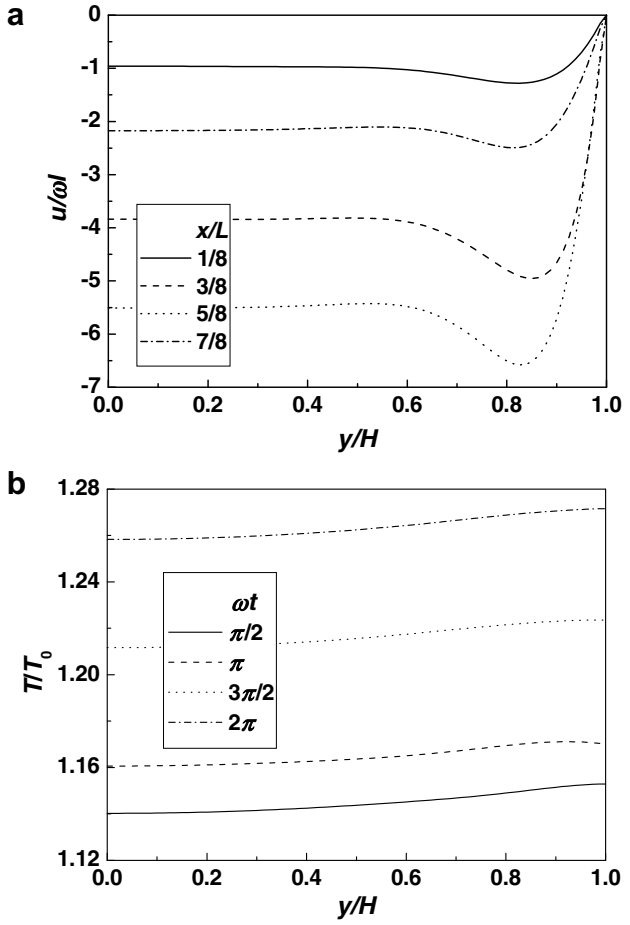

Fig. 12. (a) Velocity profiles at $\omega t = 2\pi$ and various cross sections and (b) development of temperature profiles at $x/L = 0.625$ with adiabatic walls. $\omega/\Omega = 1$, $99 \leqslant tc_s/2L \leqslant 100$.

that the temperature variations along the y direction are small for the adiabatic case.

Finally, the standard LBM (including the model used in this work) is generally considered to be applicable in the low Mach number range, so it is limited to flows where the density variation is small compared to the mean density, and the influence of the velocity field by the temperature field is negligible. To simulate the compressible flows by recovering the gas equation of state into the LBM model is important and urgent in the further extension of this work. Further investigations of the resonant tube and a more complex thermoacoustic refrigerator with compressible LBM model are underway in our group.

5. Conclusion

In this paper, numerical simulations are performed for gas resonant oscillation phenomena in a two-dimensional closed tube composed by two parallel plates using the lattice Boltzmann method. A multi-distribution function model of thermal lattice Boltzmann method devised by He et al. is introduced and adopted in this work. Both isothermal and adiabatic walls of the closed tube are considered. Boundary treatments such as moving adiabatic boundary are given in detail.

In simulations, the closed tube is driven by an oscillating plane piston at one end in the neighborhood of the fundamental resonant frequency of the gas column. The time dependent velocity, density and temperature at various locations of the tube for various frequencies and wall boundary conditions are presented. For both isothermal and adiabatic cases, shock waves are numerically captured when the oscillating plane piston at the resonant frequency or slightly off-resonant frequencies. In particular, for the isothermal case, periodically steady state of the gas-filled in the tube is reached rapidly over an initial period, and the gas oscillations are visible especially for the frequencies close to resonance. Annular effects both in velocity and temperature profiles are observed. For the adiabatic case, the state of the gas remains essentially periodically unsteady, the periodically averaged temperatures increase with the increase of the time, and the increase speed relates to the oscillation frequency. Annual effects also exist in the velocity profiles, and the temperature variations along the vertical direction are small for the adiabatic case. The gas flow and heat transfer characteristics obtained from the numerical simulations are consistent qualitatively with those from previous simulations using conventional numerical methods. Study for the gas resonance oscillations with compressible LBM model will be our further extension of the present work.

From this study, it can be concluded that the LBM can be used to obtain streaming and heat transferring patterns for the resonant oscillating flow in a tube, and it will be a promising method to investigate more complex phenomena such as the self-excited oscillations in thermoacoustic engine.

Acknowledgements

The present work was supported by the National Natural Science Foundation of China (Nos. 50425620 and

50629601) and the Specialized Research Fund for the Doctoral Program of Higher Education (No. 20050698036). Computations were performed at the National High Performance Computing Center (Xi'an).

References

[1] G. McNamara, G. Zanetti, Use of the Boltzmann equation to simulate lattice-gas automata, Phys. Rev. Lett. 61 (1988) 2235–2332.
[2] S. Succi, Lattice Boltzmann equation for fluid dynamics and beyond, first ed., Clarendon, Oxford, 2001, pp. 40–43.
[3] S.Y. Chen, G.D. Doolen, Lattice Boltzmann method for fluid flows, Annu. Rev. Fluid. Mech. 30 (1998) 329–364.
[4] R.A. Saenger, G.E. Hudson, Periodic shock waves in resonating gas columns, J. Acoust. Soc. Am. 32 (1960) 961–971.
[5] A. Alexeev, C. Gutfinger, Resonance gas oscillations in closed tubes: numerical study and experiments, Phys. Fluids 15 (11) (2003) 3397–3408.
[6] R. Betchov, Nonlinear oscillations of a column of gas, Phys. Fluids 1 (1958) 205–212.
[7] W. Chester, Resonant oscillations in closed tubes, J. Fluid Mech. 18 (1964) 44–64.
[8] M.A. Ilgamov, R.G. Zaripov, R.G. Galiullin, V.B. Repin, Nonlinear oscilltions of a gas in a tube, Appl. Mech. Rev. 49 (3) (1996) 137–154.
[9] P. Merkli, H. Thomann, Transition to turbulence in oscillating pipe flow, J. Fluid Mech. 68 (1975) 567–576.
[10] P. Merkli, H. Thomann, Thermoacoustic effects in a resonant tube, J. Fluid Mech. 70 (1975) 161–177.
[11] A. Goldshtein, P. Vainshtein, M. Fichman, C. Gutfinger, Resonance gas oscillations in closed tubes, J. Fluid Mech. 322 (1996) 147–163.
[12] A. Gopinath, N.L. Tait, S.L. Garrett, Thermoacoustic streaming in a resonant channel: the time averaged temperature distribution, J. Acoust. Soc. Am. 103 (1998) 1388–1405.
[13] C.P. Lee, T.G. Wang, Nonlinear resonance and viscous dissipation in an acoustic chamber, J. Acoust. Soc. Am. 92 (1992) 2195–2206.
[14] L. Elvira-Segura, E. Sarabia, Numerical and experimental study of finite-amplitude standing waves in a tube at high sonic frequencies, J. Acoust. Soc. Am. 104 (1998) 708–714.
[15] A.A. Aganin, M.A. Ilgamov, E.T. Smirnova, Development of longitudinal gas oscillations in a closed tube, J. Sound Vibrat. 195 (3) (1996) 359–374.
[16] H.Z. Tang, P. Cheng, Numerical simulations of resonant oscillation in a tube, Numer. Heat Transfer, Part A 40 (2001) 37–54.
[17] J.M. Buick, C.A. Greated, D.M. Campbell, Lattice BGK simulation of sound wave, Europhys. Lett. 43 (3) (1998) 235–240.
[18] D. Haydock, J.M. Yeomans, Lattice Boltzmann simulations of acoustic streaming, J. Phys. A: Math. Gen 34 (2001) 5201–5213.
[19] D. Haydock, J.M. Yeomans, Lattice Boltzmann simulations of attenuation-driven acoustic streaming, J. Phys. A: Math. Gen. 36 (2003) 5683–5694.
[20] X.M. Li, R.C.K. Leung, R.M.C. So, One-step aeroacoustics simulation using lattice Boltzmann method, AIAA J. 44 (1) (2006) 78–89.
[21] A. Bartoloni, C. Battista, S. Cabasino, et al., LBE simulations of Rayleigh-Bénard convection on the APE100 parallel processor, Int. J. Mod. Phys. C 4 (1993) 993–1006.
[22] X.Y. He, S.Y. Chen, G.D. Doolen, A novel thermal model for the lattice Boltzmann method in incompressible limit, J. Comput. Phys. 146 (1998) 282–300.
[23] Z.L. Guo, B.C. Shi, C.G. Zheng, A coupled lattice BGK model for the Boussinesq equations, Int. J. Numer. Methods. Fluids 39 (2002) 325–342.
[24] A. D'Orazio, S. Succi, C. Arrighetti, Lattice Boltzmann simulation of open flows with heat transfer, Phys. Fluids 15 (9) (2003) 2778–2781.
[25] G.H. Tang, W.Q. Tao, Y.L. He, Thermal boundary condition for the thermal lattice Boltzmann equation, Phys. Rev. E 72 (2005) 016703: 1–016703:6.
[26] Y. Wang, Y.L. He, G.H. Tang, W.Q. Tao, Simulation of two-dimensional oscillating flow using the lattice Boltzmann method, Int. J. Mod. Phys. C 17 (5) (2006) 615–630.
[27] H.N. Dixit, V. Babu, Simulation of high Rayleigh number natural convection in a square cavity using the lattice Boltzmann method, Int. J. Heat Mass Transfer 49 (2006) 727–739.
[28] C.K. Chen, T.S. Yen, Y.T. Yang, Lattice Boltzmann method simulation of backward-facing step on convective heat transfer with field synergy principle, Int. J. Heat Mass Transfer 49 (2006) 1195–1204.
[29] G. McNamara, B. Alder, Analysis of the lattice Boltzmann thermodynamics, Physica A 194 (1993) 218–228.
[30] G. McNamara, B. Alder, A hydrodynamically correct thermal lattice Boltzmann model, J. Stat. Phys. 87 (1997) 1111–1121.
[31] Y. Chen, H. Ohashi, M. Akiyama, Thermal lattice Bhatanagar–Gross–Krook model without nonlinear deviations in macrodynamic equations, Phys. Rev. E 50 (4) (1994) 2776–2783.
[32] A. D'Orazio, S. Succi, Simulating two-dimensional thermal channel flows by means of a lattice Boltzmann method with new boundary conditions, Future Gener. Comp. Sy. 20 (2004) 935–944.
[33] Z.L. Guo, C.G. Zheng, B.C. Shi, Non-equilibrium extrapolation method for velocity and boundary conditions in the lattice Boltzmann method, Chin. Phys. Soc. 11 (4) (2002) 0366–0374.
[34] R.W. Mei, W. Shyy, On the finite difference-based lattice Boltzmann method in curvilinear coordinates, J. Comput. Phys. 143 (1998) 426–448.
[35] Y. Shi, T.S. Zhao, Z.L. Guo, Finite difference-based lattice Boltzmann simulation of natural convection heat transfer in a horizontal concentric annulus, Comp. Fluids 35 (2006) 1–15.
[36] V. Christian, C.P. Cleofe, Numerical model for nonlinear standing waves and weak shocks in thermoviscous fluids, J. Acoust. Soc. Am. 109 (6) (2001) 2660–2667.
[37] T. Kataoka, M. Tsutahara, Lattice Boltzmann model for the compressible Navier–Stokes equations with flexible specific-heat ratio, Phys. E 69 (2004) 03570:1–03570:4.